Chem

CellPress

Article

# Porous polyisothiocyanurates for selective palladium recovery and heterogeneous catalysis

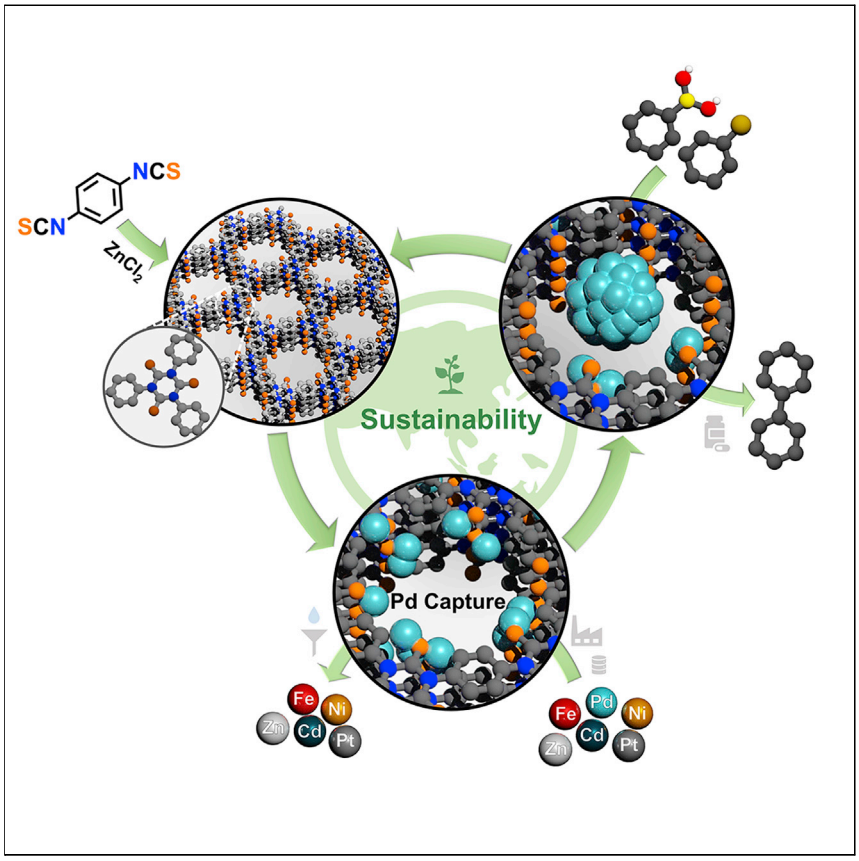


We demonstrated the synthesis of porous polyisothiocyanurates through the trimerization of commercially available 1,4-phenyldiisothiocyanate as efficient adsorbents for highly selective Pd(II) recovery from wastewater conditions. The polymers showed high surface areas and enabled simultaneous realization of a high Pd(II) adsorption capacity of 909 mg $g^{-1}$, extremely fast adsorption kinetics, and high selectivity through *in situ*-generated thiourea moieties within the hierarchically porous polymer network. Additionally, the reduction of recovered Pd(II) within the polymers led to a highly efficient heterogeneous catalyst for the Suzuki-Miyaura cross-coupling reaction.

Kyung Seob Song, Timur Ashirov, Siddulu Naidu Talapaneni, ..., Maarten Nachtegaal, Christophe Copéret, Ali Coskun

ali.coskun@unifr.ch

## Highlights

Porous polyisothiocyanurates as efficient solid sorbets for Pd capture

Highly selective recovery of Pd from wastewater under practical conditions

The highest Pd uptake capacity of 909.1 mg $g^{-1}$ and fast adsorption kinetics

Recovered Pd used as a heterogeneous catalyst for cross-coupling reactions

Song et al., Chem *8*, 1–17
July 14, 2022 © 2022 Elsevier Inc.
https://doi.org/10.1016/j.chempr.2022.05.009

Please cite this article in press as: Song et al., Porous polyisothiocyanurates for selective palladium recovery and heterogeneous catalysis, Chem (2022), https://doi.org/10.1016/j.chempr.2022.05.009

Chem

CellPress

Article

# Porous polyisothiocyanurates for selective palladium recovery and heterogeneous catalysis

Kyung Seob Song,[1,2] Timur Ashirov,[1] Siddulu Naidu Talapaneni,[3] Adam Hugh Clark,[4] Alexander V. Yakimov,[5] Maarten Nachtegaal,[4] Christophe Copéret,[5] and Ali Coskun[1,2,6,*]

## SUMMARY

**Palladium is an indispensable metal due to its wide range of industrial applications. Pd refining, however, is an extremely energy-intensive process with a serious environmental impact. Thus, the selective recovery of Pd from secondary sources is rather important. In this direction, solid sorbents are promising candidates owing to their reusability. Here, we report the synthesis of porous polyisothiocyanurates through the trimerization of 1,4-phenyldiisothiocyanate under ionothermal conditions, named covalent isothiocyanurate frameworks (CITCFs), bearing *in situ* generated thiourea moieties as binding sites for Pd. High surface area of CICTFs, 1,589 $m^2 g^{-1}$, along with the presence of abundant sulfur atoms within a hierarchically porous network, enabled an exceptional Pd(II) uptake capacity of 909 mg $g^{-1}$, fast adsorption kinetics, stable uptake over a wide pH range, and selective Pd(II) recovery from wastewater conditions. Moreover, the reduction of recovered Pd(II) within the polymer network led to highly efficient heterogeneous catalysis for the Suzuki-Miyaura cross-coupling reaction.**

## INTRODUCTION

Platinum group metals (PGMs)—namely, platinum, palladium, rhodium, ruthenium, iridium, and osmium—are precious metals with broad range of electronic,[1] industrial, and medical[2] applications. PGMs sustain high physicochemical stability and unique catalytic properties, thus making them indispensable in chemical industry, most notably in automobile catalytic converters.[3,4] Moreover, Pd has been used as a key catalyst for various cross-coupling reactions such as Suzuki, Sonogashira, Heck, Negishi, Stille, and Buchwald-Hartwig reactions.[5–8] Pd also plays a critical role as a catalyst in the hydrogen evolution reaction (HER), in hydrogen storage and purification.[9,10] Considering the massive demand for Pd, mining alone is not sufficient to produce enough supply as the Pd concentration in the ore is very low (<10 g/ton) compared with the other transition metals; thus, the recovery of Pd from new and old scrap is needed. Moreover, the cost of Pd is much higher than those of Au and Ag, thus making it a very attractive target.[11] Pd refining is a highly energy intensive process, involving multistep heating cycles, e.g., electric arc furnace operating at temperatures of 1,450°C.[12] Thus, this process has a serious environmental impact due to the significant $CO_2$ emissions, estimated 3.88 tons per 1 kg of Pd.[12,13] In this sense, Pd recovery from secondary sources including waste electronics, used catalysts, and high-level liquid waste (HLLW) from spent nuclear fuel has become an important research topic to keep up with the high demand.[14] Liquid-liquid extraction is the most widely applied technique for Pd recovery.[14] In this process, the extractant molecules bearing nitrogen, sulfur,[15] phosphorous, and/or oxygen donor

### The bigger picture

Platinum group metals (PGMs) are highly important for many industrial applications due to their stability and unique catalytic applications. However, refining these metals is a highly energy-intensive process resulting in a serious environmental impact. For the sustainable production of these metals, their recovery from new and old scrap is essential. In this direction, the reusability and high stability of solid sorbents present significant advantages over the liquid-liquid extraction approach. Sorbents bearing sulfur atoms (soft base) could be ideal candidates for the selective recovery of PGMs (soft acids) such as Pd. In this study, we report porous polyisothiocyanurates bearing *in situ*-generated thiourea binding sites as sorbents for Pd(II) combining high uptake capacity, fast kinetics, and stability under acidic conditions with high selectivity and as ideal hosts for Pd nanoparticles to form highly efficient heterogeneous catalysts for the Suzuki-Miyaura cross-coupling reaction.

Please cite this article in press as: Song et al., Porous polyisothiocyanurates for selective palladium recovery and heterogeneous catalysis, Chem (2022), https://doi.org/10.1016/j.chempr.2022.05.009



atoms[16] form coordination complexes with Pd in the biphasic acidic water/organic solvent system.[17,18] In order to improve Pd extraction and the solubility of the Pd-complex in the organic phase, generally, diluents such as n-dodecane are used. Following the saturation of the organic phase, back extraction from organic phase is performed for Pd recovery.[14] It should be noted that Pd extraction performance/capacity highly depends on the pH, counter ions ($NO_3^{2-}$ and $Cl^-$), as well as aromatic or paraffinic diluents (e.g., n-dodecane and benzene). Moreover, the economic viability of the syntheses of extractants, their stability under harsh conditions (e.g., strong acid treatment), as well as the solubility of extractants in the organic phase, which significantly decreases the yield of metal precipitation, are still important concerns.

Solid adsorbents offer significant advantages for Pd recovery compared with the liquid-liquid extraction—namely, (1) organic solvent is not required to extract Pd(II) cations, (2) high stability, (3) easy separation (solid-liquid phase), and (4) reusability. In this direction, a classical synthetic approach is to introduce nitrogen functionalities as chelating sites for Pd(II) onto a polymer backbone or a porous support. Accordingly, porous materials such as activated carbon, polymeric resins,[19] polystyrene beads, silica, metal organic frameworks (MOFs),[20] and porous organic polymers (POPs)[21–24] have already been explored as solid adsorbents for Pd(II).[25] However, the simultaneous realization of high adsorption capacity, fast adsorption kinetics, high Pd selectivity over other metals, in particular, Pt and Rh, as well as the facile reusability remain as a critical challenge in solid adsorbents, which require rational design of bindings sites as well as control over textural properties.

POPs have enjoyed a burgeoning interest in recent years due to their modular synthesis, control over chemical functionalities, high surface areas, and physicochemical stabilities.[26] POPs have already found applications in gas capture,[27,28] heterogeneous catalysis,[29,30] and environmental remediation.[31–33] Few examples of POPs featuring nitrogen functionalities toward the recovery of PGMs were elegantly demonstrated by Yavuz and Ma.[21,24] We reasoned that sulfur-rich POPs could be better suited for Pd capture due to the strong interaction between a sulfur atom, a soft base, and PGMs, soft acids. In fact, sulfur-containing functional groups such as thiourea, thiol, mercaptobenzimidazole, and mercaptobenzothiazole have already been applied for Pd capture.[34] In particular, thiourea is the most popular one due to its low-cost and high affinity toward Pd.[35] Accordingly, here, we report the synthesis of porous polyisothiocyanurates, named covalent isothiocyanurate frameworks (CITCFs), through the trimerization of commercially available 1,4-phenyldiisothiocyanate under ionothermal conditions using molten $ZnCl_2$ as a reactive solvent. The trimerization reaction of isothiocyanate molecules is an atom-efficient, practical, and scalable route for the synthesis of polyisothiocyanurates bearing *in-situ* generated thiourea moieties as binding sites for Pd(II). High surface area of polyisothiocyanurate network increases the accessibility of binding sites for Pd(II) uptake. Moreover, polyisothiocyanurates also offer high thermal and chemical stabilities, which are critical for their application for efficient Pd(II) capture under harsh acidic conditions and for the subsequent utilization of captured Pd within the polymer network as a heterogeneous catalyst for the Suzuki cross-coupling reaction.

## RESULTS

### Structural and porosity characterizations of CITCFs

Having recognized that the molar ratio of $ZnCl_2$ and the reaction temperature have a profound impact on the heteroatom content, crystallinity, and the porosity of POPs synthesized under ionothermal conditions,[36,37] we varied (Figure 1) both the

[1]Department of Chemistry, University of Fribourg, Fribourg 1700, Switzerland

[2]National Centre of Competence in Research (NCCR) Catalysis, University of Fribourg, Fribourg 1700, Switzerland

[3]Australian Carbon Materials Centre (A-CMC), School of Chemical Engineering, University of New South Wales (UNSW), Sydney, NSW 2052, Australia

[4]Laboratory for Synchrotron Radiation and Femtochemistry (LSF), Paul Scherrer Institute, Forschungsstrasse 111, 5232 Villigen, Switzerland

[5]Department of Chemistry and Applied Biosciences, ETH Zürich, Vladimir-Prelog-Weg1–5, CH-8093 Zürich, Switzerland

[6]Lead contact

*Correspondence: ali.coskun@unifr.ch

https://doi.org/10.1016/j.chempr.2022.05.009

Please cite this article in press as: Song et al., Porous polyisothiocyanurates for selective palladium recovery and heterogeneous catalysis, Chem (2022), https://doi.org/10.1016/j.chempr.2022.05.009





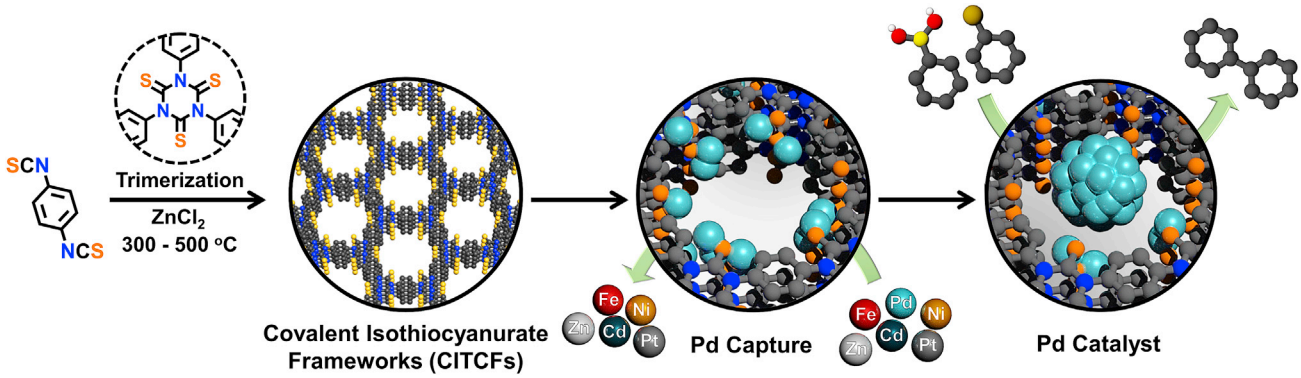


**Figure 1. Synthetic pathway for the preparation CITCFs and their applications**

Graphical representations of the proposed structure of CITCFs along with the demonstration of selective Pd(II) recovery from the mixtures of transition metals and Pt(IV) under highly acidic conditions. The reduction of captured Pd(II) within CITCF-500 to form a highly efficient heterogeneous catalyst for the Suzuki-Miyaura cross-coupling reaction.

reaction temperature (300°C, 400°C, and 500°C) and the $ZnCl_2$ amount (2.5, 5 and 10 equiv) in the synthesis of CITCFs and comparatively analyzed their structural and textural properties (see experimental procedures; Figures S1–S7; Tables S1 and S2). Surface area screening results revealed (Figures S1 and S6; Tables S1 and S2) consistently higher values for the CITCFs synthesized using 5 equiv of $ZnCl_2$, which were used for further analysis.

In order to verify the formation of isothiocyanurate rings under ionothermal conditions, we synthesized 1,3,5-triphenyl-1,3,5-triazine-2,4,6-trithione (model compound 1) and 1,3,5-tri([1,1′-biphenyl]-4-yl)-1,3,5-triazine-2,4,6-trithione (model compound 2) as model compounds starting from phenylisothiocyanate and 4-biphenyl isothiocyanate, respectively (Scheme S1). Although the model compound 1 was obtained in a rather low yield due to the low boiling point of the monomer (below the melting point of the salt), model compound 2 was isolated in a 54% yield. Both compounds were fully characterized by nuclear magnetic resonance (NMR) spectroscopy and high-resolution mass analyses, thus verifying the formation of isothiocyanurate rings under ionothermal conditions (Figures S8–S13). The formation of CITCFs was probed by Fourier transform infrared spectroscopy (FTIR) analysis (Figure 2A). We compared (Figure S14) the FTIR spectra of model compound 1, 2, and CITCFs synthesized at 300°C, 400°C, and 500°C to probe the formation of isothiocyanurate rings. Thiocarbonyl derivatives (R–N–C=S) have three characteristic FTIR bands—namely, band I at 1,395–1,570 $cm^{-1}$ for N–R, band II at 1,260–1,420 $cm^{-1}$ for C–N, and band III at 940–1,140 $cm^{-1}$ for C=S stretching.[38,39] Both model compounds showed these characteristic bands. In the case of CITCFs, we also observed these bands albeit with a blue-shift in band I and a red-shift in bands II and III, thus verifying the formation of isothiocyanurate rings and the formation of CITCFs. Elemental analysis of CITCFs (Tables 1 and S3) showed the depletion of sulfur and higher carbon contents with increasing reaction temperature, pointing to the irreversible side reactions and partial carbonization. Similar phenomenon is also observed for covalent triazine frameworks (CTFs).[37] Nevertheless, up to 14.6 wt% of nitrogen and 13.9 wt% of sulfur can be preserved for CITCF-500. We also conducted thermogravimetric analysis (TGA) to probe thermal stability of CITCFs. TGA analysis showed (Figure S15) ~10% mass loss up to ~150°C arising from the loss of water and residual solvents from the network. The TGA curves of CITCF-300, CITCF-400 and CITCF-500 showed thermal stabilities up to ~400°C. Moreover, TGA curves obtained under air did not show any residual mass proving the complete

Please cite this article in press as: Song et al., Porous polyisothiocyanurates for selective palladium recovery and heterogeneous catalysis, Chem (2022), https://doi.org/10.1016/j.chempr.2022.05.009



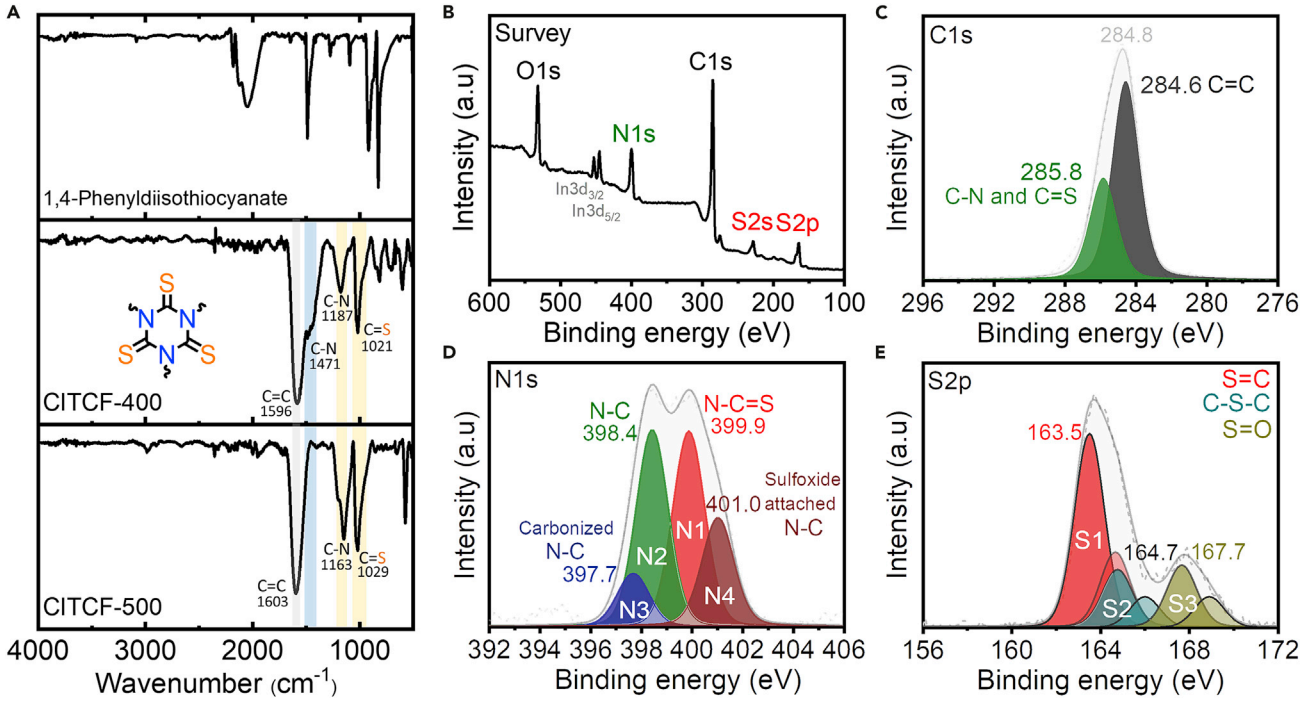


**Figure 2. Structural characterization of CITCFs**

(A) FTIR spectra of 1,4-phenyldiisothiocyanate, CITCF-400, and CITCF-500. The disappearance of N=C=S stretching vibration of 1,4-phenyldiisothiocyanate at 2,054 $cm^{-1}$ and the emergence of characteristic isothiocyanurate ring stretching vibrations can be observed at 1,188 and 1,593 $cm^{-1}$ for CITCFs.

(B–E) (B) XPS survey spectrum, (C) C 1s, (D) N 1s, and (E) S 2p XPS spectra of CITCF-500.

removal of inorganic species (Figure S15A). Additionally, we also performed Raman analysis and observed the characteristic D and G bands for CITCFs (Figure S16; Table S4) at 1,346.1 and 1,546.5 $cm^{-1}$, respectively. We also observed the 2D band at 2,950 $cm^{-1}$, which is commonly observed in 2D carbon-based materials.[40] In agreement with the EA results, Raman spectra also revealed partial carbonization in the CITCFs as the $I_D/I_G$ ratio increased with the reaction temperature, 0.62, 0.94, and 1.03 for CITCF-300, CITCF-400, and CITCF-500, respectively.

X-ray photoelectron spectroscopy (XPS) analysis was performed to further clarify the nature of chemical bonding in CITCFs and compared with the XPS spectrum of model compound 1 (Figures 2B–2E, S17, and S18). The deconvolution of C1s peak in the XPS spectrum of model compound 1 showed two peaks assigned to C=C at 284.6 eV and C=N/C=S at 285.8 eV (Figure S18A). The deconvoluted N1s peak also showed two peaks at 401.2 and 400.6 eV originating from N–C=S and N–C, respectively (Figure S18B). Moreover, S2p spectrum showed two peaks for $S2p_{3/2}$ at 163.1 eV and $S2p_{1/2}$ at 164.3 eV (Figure S18C). These binding energies were found to be higher than those of thiourea and thione derivatives. The XPS survey spectra of CITCF-300, CITCF-400, and CITCF-500 (Figures S17B, S17C, and S17D) exhibited only C1s, N1s, O1s, and S2p peaks without any other inorganic residues. C1s XPS spectra of CITCFs (Figures S18D, S18G, and S18J) were found to be similar to that of model compound 1 (Figure S18A). The deconvoluted N1s XPS spectra of CITCFs (Figures S18E, S18H, and S18K) showed the same peaks to those of model compound 1 for N–C=S and N–C (Figure S18B). However, we observed an additional peak at 397.5 eV, which is attributed to the partial carbonization of the polymer network and consistently observed for all the CITCFs. Moreover, the

Please cite this article in press as: Song et al., Porous polyisothiocyanurates for selective palladium recovery and heterogeneous catalysis, Chem (2022), https://doi.org/10.1016/j.chempr.2022.05.009





**Table 1. BET surface area and elemental analysis of CITCFs**

| Sample | BET[a], ($m^2\ g^{-1}$) | Langmuir, ($m^2\ g^{-1}$) | $S_{micro}$[b] ($m^2\ g^{-1}$) | $S_{ext}$ ($m^2\ g^{-1}$) | $V_{total}$[c] ($cm^3\ g^{-1}$) | $V_{micro}$[d] ($cm^3\ g^{-1}$) | $d_{micro}$[e] (nm) | Elemental analysis (wt%) | | | |
|---|---|---|---|---|---|---|---|---|---|---|---|
| | | | | | | | | C | N | H | S |
| | | | | | | | | 48.95[f] | 14.27[f] | 4.11[f] | 32.67[f] |
| CITCF-400 | 780 | 929 | 581 | 198 | 0.41 | 0.2 | 0.47 | 55.2 | 14.2 | 1.0 | 17.5 |
| CITCF-500 | 1,589 | 1,901 | 772 | 817 | 0.89 | 0.25 | 0.47 | 58.0 | 14.6 | 0.6 | 13.9 |

[a]BET surface area calculated over the pressure range ($P/P_0$) obtained from Rouquerol plots.
[b]Micropore surface area calculated from the adsorption isotherm using the *t*-plot method.
[c]Total pore volume obtained at $P/P_0 = 0.99$.
[d]Micropore volume calculated using the *t*-plot method.
[e]Micropore diameter calculated from NLDFT method.
[f]Theoretical values calculated for $C_{24}H_{24}N_6S_6$.

presence of an additional peak at 401 eV in the case of CITCF-500 was attributed to the partial oxidation of sulfur atoms. Importantly, the deconvoluted S2p spectra of CITCFs (Figures S18F, S18I, and S18L) revealed apparent isothiocyanurate ring structure even at high reaction temperatures. We also observed cyclic sulfur species, C–S–C at 164.6 eV ($S2p_{3/2}$) and 165.8 ($S2p_{1/2}$) for all the CITCFs, pointing to partial carbonization and also providing information on the nature of sulfur species within the structure. This binding energy overlaps nicely with reported heterocyclic thione derivatives,[41,42] i.e., mecaptobenzothiazole shows the endo type S–C bond at 164.8 eV ($S2p_{3/2}$) and 166.0 eV ($S2p_{1/2}$).[42] We observed an additional peak in the S2p spectrum of CITCF-500 at 167.7 eV, which was assigned to oxidized sulfur species and could form through the reaction of sulfur with trapped water molecules (Figures S18L and 2E). The comparative analysis of XPS data clearly demonstrated the formation of CITCFs, the retention of isothiocyanurate rings even at high reaction temperatures, and the partial carbonization of the polymer structure.

In order to gain further insights into the structure of CITCFs, multinuclear ($^1H$, $^{13}C$ and $^{15}N$) solid-state NMR studies were conducted (Figures S19–S21). $^1H$ magic-angle spinning (MAS) NMR spectra for CITCF-300, CITCF-400, and CITCF-500 (Figure S19A) showed two sets of signals: a broad feature at ~7–8 ppm and an array of narrow signals between ~0 and 3 ppm. The former one can be assigned to the aromatic moieties, which showed a downfield shift upon increasing the synthesis temperature. The latter ones are tentatively assigned to the protons of adsorbed water (*vide infra*) constrained within the CITCF structure; the very narrow lines indicating that the protons are very isolated and yet relatively strongly interacting with the polymer backbone. Additionally, the fast dynamics within water molecules can contribute to the linewidth. This proposal is corroborated by the 2D $^1H$ single-quantum double-quantum (SQ-DQ) correlation NMR (Figure S19B) on CITCF-500, where only self-correlating $^1H$ signals are observed, consistent with their attribution to adsorbed water. In addition, the $^1H$-$^{13}C$ CP/MAS NMR spectra (Figure S20) of CITCFs showed three sets of signals: a broad and intense feature centered at ~130 ppm associated with the aromatic moiety along with the one at 148 ppm, which is consistent with what is expected for C–N carbon. Noteworthy, no pronounced signal corresponding to C=S expected at 170–180 ppm was observed, which was most likely related to low polarization transfer efficiency to tertiary carbon in C=S as well as the partial carbonization of CITCF as verified by the EA, Raman, and XPS analyses. Notably, the $^{13}C$ NMR spectra of CITCFs were found to be in a good agreement with that of model compound 1. Although $^{15}N$ MAS NMR studies for the materials with natural $^{15}N$ abundance is precluded in normal conditions by the receptivity

Please cite this article in press as: Song et al., Porous polyisothiocyanurates for selective palladium recovery and heterogeneous catalysis, Chem (2022), https://doi.org/10.1016/j.chempr.2022.05.009



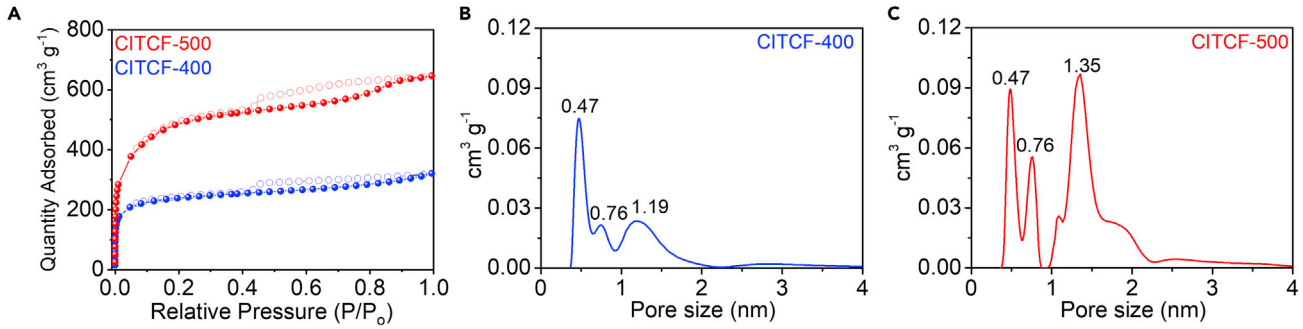


**Figure 3. BET surface area and pore size distribution analyses of CICTFs**

(A) Ar adsorption (filled) and desorption (empty) isotherms at 77 K for CITCF-400 (blue) and CITCF-500 (red).

(B and C) NLDFT pore size distribution plots (B) CITCF-400 and (C) CITCF-500. Both CITCF-400 and CITCF-500 showed similar pore sizes of in the ultramicropore range (< 0.7 nm); however, CITCF-500 showed pore widening and higher pore volume compared with CITCF-400.

and low-gamma of $^{15}N$, dynamic nuclear polarization-enhanced[43] $^{1}H$-$^{15}N$ CP/MAS NMR (Figure S21) provided a sensitivity enhancement of 4.3 on CITCF-500 and enabled to observe relatively broad feature at ~145 ppm that was attributed to the nitrogen inside the CITCF structure.

Powder X-ray diffraction (PXRD) analysis was conducted to investigate the crystallinity of CITCFs (Figure S7). CITCFs were found to be amorphous and showed a broad diffraction peak at $2\theta = 25.7°$, which is attributed to 001 basal plane diffraction peak, suggesting the existence of graphitic layers with a d-spacing of 3.4 Å.[44] Scanning electron microscopy (SEM) analysis (Figures S22 and S23) of CITCFs revealed irregular shaped micron-sized particles. We observed smaller particles for CITCF-500 along with the formation of a highly porous surface morphology.

In order to investigate the textural properties of CITCFs, Ar adsorption-desorption isotherms were measured at 77 K (Figure 3A; Table 1). CITCF-400 and CITCF-500 showed Brunauer-Emmett-Teller (BET) surface areas of 780 and 1,589 $m^2\,g^{-1}$ along with the total pore volumes of 0.41 and 0.89 $cm^3 \cdot g^{-1}$, respectively. Consistent with the POPs synthesized under ionothermal conditions,[37] increasing the reaction temperature led to an increase in the mesopore content, thus forming a hierarchical pore network. Both CITCF-400 and CITCF-500 showed type I isotherms and H4 hysteresis loop in the desorption branch at about $P/P_o = 0.4$, pointing to the coexistence of abundant micropores and mesopores. Nonlocal density functional theory (NLDFT) method was used (Figures 3B and 3C) to determine the pore size distribution of CITCFs. Although both CITCF-400 and CITCF-500 showed ultramicropores (below 0.7 nm), we also observed larger pores for the CITCF-500 with micropores up to 1.35 nm. Additionally, Barrett, Joyner, and Halenda (BJH) pore size analysis of CITCF-500 revealed broad range of mesopores from 5 to 20 nm, thus verifying the presence of a hierarchical porous network, which is beneficial for efficient mass transport.

## Palladium capture under wastewater conditions

High surface area, sulfur content, hierarchical porosity, reusability, and chemical stability of CITCF-500 present unique advantages over sulfur-based extractants and adsorbents to capture Pd(II) under harsh wastewater conditions. In order to determine the maximum Pd(II) uptake capacity of CITCF-500, 5 mg of CITCF-500 was added to the 10 mL of 800 ppm Pd(II) solution and stirred for 24 h until the equilibrium concentration is reached, which was then analyzed using inductively coupled plasma optical emission spectrometry (ICP-OES). CITCF-500 showed an exceptional Pd(II) uptake

Please cite this article in press as: Song et al., Porous polyisothiocyanurates for selective palladium recovery and heterogeneous catalysis, Chem (2022), https://doi.org/10.1016/j.chempr.2022.05.009





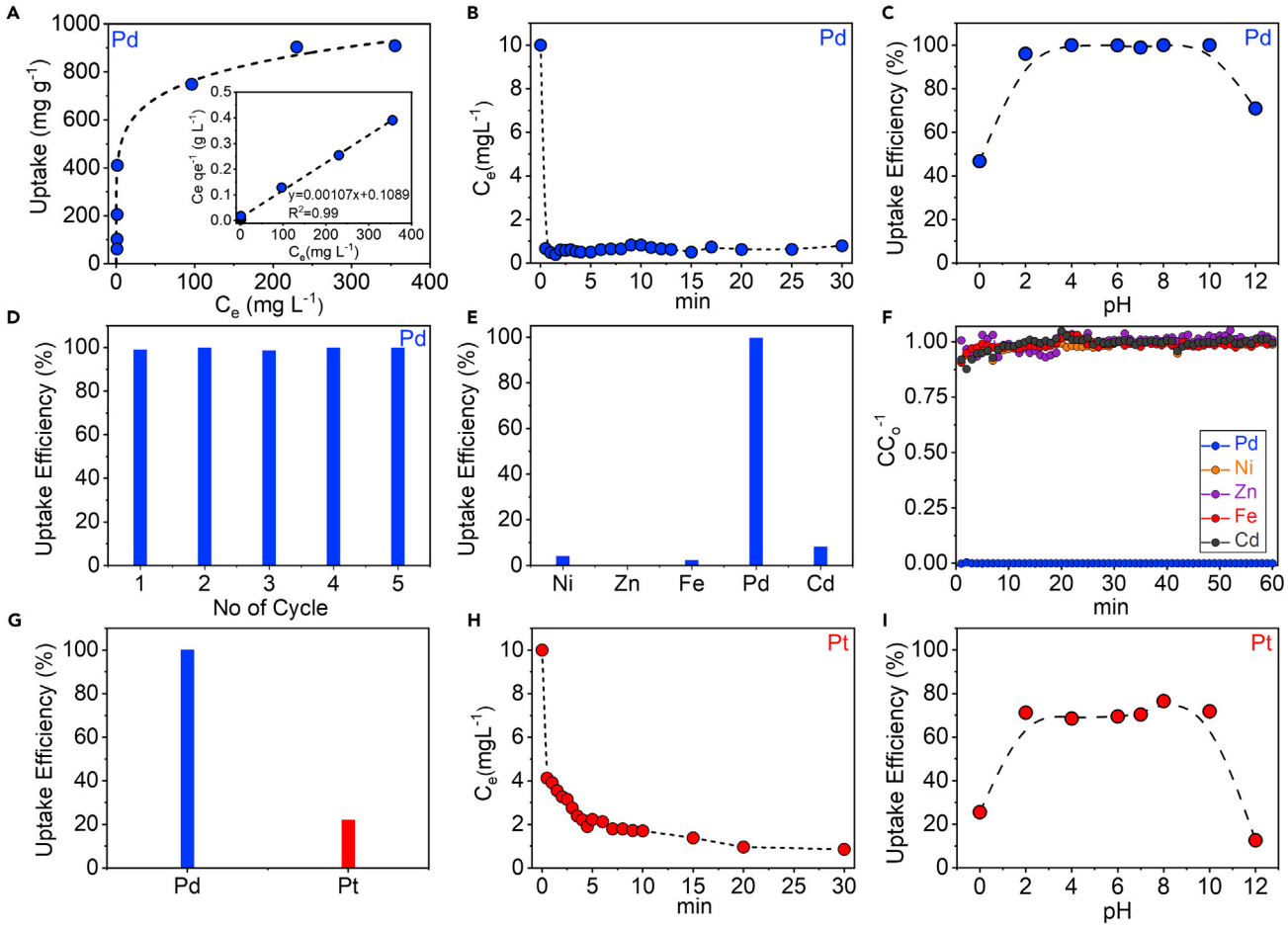


**Figure 4. Pd(II) capture and recovery performance of CITCF-500**

(A) Pd(II) uptake isotherm of CITCF-500. The uptake isotherm was fitted with a Langmuir adsorption model (inset).

(B) Pd(II) adsorption kinetics of CITCF-500. Fast Pd(II) uptake kinetics show the high Pd(II) affinity of CITCFs.

(C) pH dependency of Pd(II) uptake efficiency.

(D) Reusability of CITCF-500 for Pd(II) recovery over five cycles without any performance loss.

(E) Selective Pd(II) capture from wastewater containing mixture of transition metal ions.

(F) Breakthrough experiment of CITCF-500 using a wastewater conditioned mixture.

(G) Selective Pd(II) capture from a Pd(II)/Pt(IV) mixture at pH 0.

(H) Pt(IV) adsorption kinetics, (I) pH dependency of Pt(IV) uptake efficiency. The CITCFs exhibit high selectivity toward Pd(II) over other metals ions.

capacity of 929 mg $g^{-1}$ owing to the presence of well-defined isothiocyanurate rings as well as the high surface area of CITCF-500. Pd(II) adsorption isotherm was obtained by measuring the equilibrium uptake capacity of CITCF-500 at various Pd(II) concentrations ranging from 3.6 to 500 ppm. Pd(II) adsorption isotherm of CITCF-500 was fitted with Langmuir and Freundlich models (see Figures 4A, S24, and S25). Adsorption capacity ($Q_m$) from the Langmuir equation was found to be 909 mg $g^{-1}$ (Figure S24), which is the highest value reported to date (see Table S5). In particular, $R^2$ value of 0.99 from Langmuir model fitting points to the homogeneous monolayer adsorption of Pd(II) based on the Langmuir theory, which is attributed to the well-distributed sulfur atoms in the CITCF-500 structure.

We also performed kinetic analysis to probe the Pd(II) capture performance of CITCF-500 (Figure 4B). Accordingly, 10 ppm Pd(II) solution (200 mL) was prepared and 5 mg of CITCF-500 was added to this solution. Several data points were

Please cite this article in press as: Song et al., Porous polyisothiocyanurates for selective palladium recovery and heterogeneous catalysis, Chem (2022), https://doi.org/10.1016/j.chempr.2022.05.009



obtained from 0 to 30 min by using ICP-OES to measure remaining Pd(II) in the solution and to probe the change in the concentration over time. This kinetic Pd(II) isotherm was fitted (Figure S26) with pseudo-second order model[41] ($R^2$=1.00) and $k$ value for Pd(II) was calculated to be $3.26 \times 10^{43}$, which is substantially higher than those of sulfur functionalized adsorbents (see Table S5). Notably, it took only 30 s to adsorb 99% of Pd(II) ions in the solution, which shows extremely high affinity of CITCF-500 toward Pd(II). It is also important to note that hierarchical porosity of CITCF-500 improves the mass-transfer and contributes to the rapid Pd(II) uptake through the nanoconfinement effect.[24,45] Based on this kinetic data, we also calculated the distribution coefficient ($K_d$), that is $5.6 \times 10^5$ for Pd(II) (Figure S27), pointing to the strong binding between isothiocyanurate sites and Pd(II) ions. Higher affinity compared with thiourea was attributed to the presence of highly preorganized binding sites within CITCF-500. Pd(II) adsorption performance of sorbents highly depends on the pH of the solution. Accordingly, we tested (Figure 4C) Pd(II) adsorption performance of CITCF-500 in the wide pH range of 0–12. Interestingly, CITCF-500 showed a stable Pd(II) adsorption from pH 2 to 10, verifying pH independent Pd(II) uptake, which is an important parameter for practical applications when considering the fact that waste electronics and used catalysts are treated with strong acids such as HCl.[7] Moreover, CITCF-500 also showed (Figure 4D) a good reusability with nearly 100% Pd uptake efficiency over 5 cycles.

Pd(II) adsorption mechanism of amine-based sorbents in an acidic solution occurs through anion exchange mechanism between protonated amine (i.e., $R_2NH^+Cl^-$) of adsorbent and anionic Pd(II) chlorocomplex (e.g. $2H^+PdCl_4^{2-}$).[18] Also, depending on the $Cl^-$ concentration, Pd cation forms different coordination complexes, which not only affect the Pd(II) coordination but also determine the Pd(II) capture capacity. Compared with the amine-based sorbents, sulfur-based adsorbents are less sensitive to pH.[18] In order to further elaborate on the Pd(II) binding mechanism of CITCF-500, we recorded FTIR spectra with an extended spectral region up to 220 $cm^{-1}$ (Figure S28). We observed a red shift in the trithiourea band (from 1,599 $cm^{-1}$ and 1,150 $cm^{-1}$ to 1,602 $cm^{-1}$ and 1,207 $cm^{-1}$) upon Pd coordination with isothiocyanurate moieties. Importantly, 277 $cm^{-1}$ band of Pd(II)@CITCF-500 agrees well with the (Pd-S) band of Pd thiourea complex ($[Pdtu_4Cl]_2$),[46] thus suggesting that Pd(II) capture in CITCF-500 occurs through ligand exchange mechanism. We also conducted XPS analysis of Pd(II)@CITCF-500 (Figure S29). The presence of Pd3d peaks in the survey spectra (Figure S29A) clearly showed the presence of Pd(II) within CITCF-500. Compared with the XPS spectrum of CITCF-500, C1s and N1s peaks of Pd(II)@CITCF-500 exhibited minor binding energy shifts (Figures S29B and S29C, Pd(II)@CITCF-500 and Figures S18J and S18K, CITCF-500). S2p peak on the other hand showed a binding energy shift of +0.4 eV, which indicates the coordination of sulfur and Pd(II) (Figure S29D, Pd(II)@CITCF-500 and Figure S18L, CITCF-500). Moreover, Pd–S bond formation can also be observed in the Pd3d XPS spectrum of Pd(II)@CITCF-500 (Figure S29E). Notably, $Pd3d_{5/2}$ peak at 337.9 eV matched perfectly with the previously reported Pd–S complexes, i.e., 337.9 eV of $Pd(SPh)_2$[47] and did not match with either $PdCl_2$ (337.6 eV of $Pd3d_{5/2}$) or $K_2PdCl_4$ (337.7 eV of $Pd3d_{5/2}$).[48] Moreover, although oxidized sulfur species exists in CITCF-500, they did not participate in the coordination as the Pd–O bond of $PdSO_4$ at 338.7 eV for $Pd3d_{5/2}$ was not observed in the XPS Pd3d spectrum.[49] Therefore, these results suggest the capture of Pd(II) through Pd–S bond formation. We additionally performed X-ray absorption spectroscopy (XAS) to investigate the local coordination environment of Pd in Pd(II)@CITCF-500 (Figure S30). Comparison of the Pd(II)@CITCF-500 XAS spectrum with the relevant standards shows remarkable similarity of the spectrum with $PdCl_2$, which demonstrates the Pd(II) oxidation state

Please cite this article in press as: Song et al., Porous polyisothiocyanurates for selective palladium recovery and heterogeneous catalysis, Chem (2022), https://doi.org/10.1016/j.chempr.2022.05.009





with a similar average local Pd coordination environment (Figure S30A). Analysis of the Fourier transformed extended X-ray absorption fine structure (EXAFS) region (Figure S30B) shows predominantly coordination with Pd–S from the appearance of a peak centered at 1.8 Å (not phase shift corrected) with a close agreement in position compared with the $PdCl_2$ reference. The slight appearance of a shoulder toward the lower radial distance could originate from bonding with light scattering atoms. Detailed analysis of EXAFS exhibited a strong agreement with a combination of Pd–S and Pd–O interaction mode (Figures S30C and S30D), which showed (Table S6) that 2.9 $\pm$ 0.3 of S atoms and 0.8 $\pm$ 0.2 of O atoms coordinated to Pd. At higher radial distance no significant additional contributions were detected, which suggests that Pd(II) is highly dispersed within CICTFs through its strong interaction with sulfur atoms and not forming nanoparticles. Considering the absence of Pd–O bond in the the XPS analysis of Pd(II)@CITCF-500 owing to the removal water molecules under the high vacuum conditions, we reasoned that the Pd–O interaction mode in the EXAFS originated from the coordinating $H_2O$ molecules.

Exceptional Pd(II) adsorption performance of CITCF-500 inspired us to test selective Pd(II) capture from wastewater conditioned metal mixture solution containing 5 ppm of Pd(II), Ni(II), Fe(II), Zn(II), and Cd(II) ions. CITCF-500 exhibited (Figure 4E) a highly selective Pd(II) uptake performance, which is comparable, if not higher, than those of sulfur functionalized and other adsorbents. In order to probe the metal content of CITCF-500 after selective Pd(II) capture from the mixture containing 5 ppm of Pd(II), Ni(II), Fe(II), Zn(II), and Cd(II), we performed (Figure S31) energy-dispersive X-ray spectroscopy (EDX) analysis of Pd(II)@CITCF-500. EDX mapping analysis revealed the presence of well-distributed sulfur, nitrogen, and Pd atoms, whereas the other metals were not observed. In order to test the selective Pd(II) capture performance of CITCF-500 under practical conditions, we also performed breakthrough experiments (Figure 4F). Accordingly, an aqueous solution containing 5 ppm Pd(II), Ni(II), Fe(II), Zn(II), and Cd(II) was passed through a column packed with CITCF-500 powder with a flow rate of 10 mL/min at room temperature. Every 10 mL aliquot was analyzed with ICP-OES to determine the residual metal content of the solution. CITCF-500 showed an exceptional 100% Pd(II) capture performance over Ni(II), Fe(II), Zn(II), and Cd(II) even after 60 min (Figure 4F). Moreover, the measured concentration of other cations was almost identical to the stock solution.

Selective recovery of Pd(II) from PGMs such as the mixture of Pd(II) and Pt(IV) is, however, more challenging to realize due to their similar properties. Accordingly, we prepared 5 ppm Pd(II) and Pt(IV) mixture solution and varied the pH (pH [0] and [7]; Figures 4G and S32). CITCF-500 showed five times higher Pd(II) uptake efficiency over Pt(IV) (100% Pd versus 22% Pt uptake efficiency) in a highly $Cl^-$ concentrated solution (pH [0]; Figure 4G). In addition to the presence of high affinity binding sites, the high selectivity toward Pd(II) in the Pd/Pt mixture under highly acidic conditions can also be attributed to the size exclusion as the size of PGM complexes are 5.5 Å for square planar $PdCl_4^{2-}$ and 8.3 Å for octahedral $Pt(IV)Cl_6^{2-}$,[50] which are the most stable forms in HCl solution. It is suggested that smaller size of $PdCl_4^{2-}$ enables faster diffusion within the hierarchical pore network and stronger nanoconfinement effect in the micropores. In agreement with the literature,[51] we observed a decrease in the uptake capacities for Pd(II) and Pt(IV) with increasing pH (Figure S32D), likely due to the formation of neutral and hydrolyzed species of Pd(II) and Pt(IV), which are not favorable for adsorption. We observed a similar Pd(II)/Pt(IV) selectivity for the CICTF-400 to the CITCF-500 (Figures S32A and S32B). In order to further understand the origin of Pd(II) selectivity of CITCF-500 over Pt(IV), we also performed kinetic analysis of Pt(IV) uptake in CITCF-500. Pt(IV) concentration versus time isotherm

Please cite this article in press as: Song et al., Porous polyisothiocyanurates for selective palladium recovery and heterogeneous catalysis, Chem (2022), https://doi.org/10.1016/j.chempr.2022.05.009



was fitted with pseudo-second order model, and $k$ value was calculated to be $7.34 \times 10^{-3}$ g mg$^{-1}$ min$^{-1}$ (Figure S33). Notably, this value was significantly lower than that of Pd(II) ($3.26 \times 10^{43}$ g mg$^{-1}$ min$^{-1}$; Figure S26). Moreover, the time required for the 90% of Pt(IV) to be adsorbed was more than 30 min, whereas only 30 s was needed for 99% Pd(II) adsorption. We calculated the distribution coefficient ($K_d$) for Pt(IV), $5.7 \times 10^4$ mL g$^{-1}$ (Figure S34), which was also lower than that of Pd(II). Furthermore, we also studied the dependency of Pt(IV) adsorption performance in the pH range of 0–12 (Figure 4I). Interestingly, CITCF-500 showed 80% uptake efficiency with a stable Pt(IV) adsorption, which was also lower than the Pd(II) uptake efficiency in the same pH range (Figure 4C). We additionally tested (Figure S35) the Pd(II) uptake performance using equimolar concentrations of the Pd(II) and Pt(IV), 0.05 mM 10 mL. Although the Pt(IV) uptake efficiency increased to 76.7% at pH 0, CITCF-500 still showed higher Pd(II) uptake efficiency of 100% for this mixture. These results clearly indicate that higher Pd(II) selectivity of CITCF-500 is mainly governed by the faster diffusion of smaller sized $Pd(II)Cl_4^{2-}$ compared with $Pt(IV)Cl_6^{2-}$ within the hierarchical porous structure of CITCF-500, the high affinity of Pd(II) toward sulfur binding sites and the nanoconfinement effect within the micropores.

## Catalytic performance of Pd@CITCFs

Pd-based heterogeneous catalysts are of great importance due to their improved stabilities, conversion yields, and recyclability.[30,52,53] For this reason, we prepared Pd(II)@CITCF-500 with a Pd(II) content of 450 mg g$^{-1}$ (8.7 mol%) as a heterogeneous catalyst for the Suzuki-Miyaura cross-coupling reaction. First, we investigated the model reaction between 4-methyl iodobenzene and phenyl boronic acid using $K_2CO_3$ as a base in toluene/$H_2O$ mixture at 100°C under air atmosphere (Table S7; Figure S36). The amount of base was found to have a profound impact on the conversion yield as well as the product selectivity. Although 3 equiv. of base led to the formation of predominantly homocoupling product (90%) in a quantitative yield, 6 equiv. of base resulted in the 72% conversion yield and 71% selectivity toward the desired coupling product along with a 29% of homocoupling product. In order to further optimize the catalytic performance, we also prepared Pd@CITCF-500 by reducing Pd(II)@CITCF-500 using $NaBH_4$ at room temperature. Transmission electron microscopy (TEM) analysis of Pd@CITCF-500 revealed Pd NPs with an average particle size of $1.49 \pm 0.079$ nm (Figure S37), which is in a good agreement with the 1.35 nm of pore of CITCF-500 (Figure 2), pointing to the fact that CITCF is an excellent host for the Pd NPs.

Moreover, the BET surface of Pd@CITCF-500 was found to be 1,260 m$^2$ g$^{-1}$, which indicates the efficient encapsulation of Pd NPs and the accessibility of pores (Figure S38A). In order to optimize the reaction conditions for Pd@CITCF-500 (Table 2; Figure S39) in the Suzuki-Miyaura cross-coupling reaction, we first investigated a model reaction between bromobenzene and phenylboronic acid using $Na_2CO_3$ as a base and DMF/$H_2O$ mixture as a solvent at 100°C under air atmosphere. We obtained the highest conversion yield of 78% after an overnight reaction. We also investigated the substrate scope of Pd@CITCF-500 under the optimized reaction conditions. Notably, Pd@CITCF-500 showed high functional group tolerance and exhibited high yields ranging from 81.6% to 99.9% with exclusive product selectivity. We also performed recyclability tests for Pd@CITCF-500 with entry 4 (4-amino-bromobenzene and phenyl boronic acid). Remarkably, Pd@CITCF-500 retained its high catalytic activity over 5 cycles and did not show a significant surface area reduction after five catalytic cycles (Figure S38). We also studied the leaching of Pd from Pd@CITCF-500 by measuring the Pd content of solution after catalytic cycles, which was found be less than 0.05 ppm. These results verify that CITCFs can be excellent hosts for Pd as heterogeneous catalysts for the cross-coupling reactions.

Please cite this article in press as: Song et al., Porous polyisothiocyanurates for selective palladium recovery and heterogeneous catalysis, Chem (2022), https://doi.org/10.1016/j.chempr.2022.05.009





**Table 2. Catalytic performance of Pd@CITCF-500 in the Suzuki-Miyaura cross-coupling reaction**

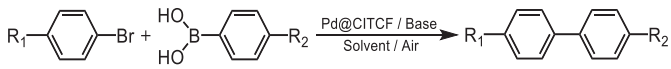


| | $R_1$ | $R_2$ | Solvent | Base | Temp (°C) | Time (h) | Yield (%)[b] |
|---|---|---|---|---|---|---|---|
| 1[a] | H | H | DMF / $H_2O$ | $Na_2CO_3$ | 100 | 16 | 78.0 |
| 2[a] | CN | H | DMF / $H_2O$ | $Na_2CO_3$ | 130 | 7 | 99.8 |
| 3[a] | $NH_2$ | H | DMF / $H_2O$ | $K_2CO_3$ | 130 | 2 | 99.0 |
| 4[a] | 4-$CH_2NO_2$ | H | DMF / $H_2O$ | $K_2CO_3$ | 130 | 2 | 81.6 |
| 5[a] | H | 4-$C_5H_4N$ | DMF / $H_2O$ | $K_2CO_3$ | 130 | 12 | 83.9 |
| 6[a] | H | 3-CHO | DMF / $H_2O$ | $K_2CO_3$ | 130 | 4 | 97.9 |
| 7[a] | H | 4-$OCH_3$ | DMF / $H_2O$ | $K_2CO_3$ | 130 | 4 | 99.9 |

[a]$R_1$-bromobenzene (0.5 mmol), $R_2$-phenyl boronic acid (0.75 mmol), base (0.75 mmol), DMF / $H_2O$ (2.5 ml/3.5 ml), air, Pd@CITCF (10 mg) with 8.7 mol% of Pd loading.
[b]Isolated yield from the halide benzene.

## DISCUSSION

We have demonstrated atom-efficient synthesis of the CITCFs through the trimerization of aromatic isothiocyanates under ionothermal condition. CITCFs showed high surface areas and hierarchical porosity with interconnected micro-, meso- and macro-pores, thus offering a versatile polymeric platform for the recovery of PGMs such Pd from new and old scrap. The presence of sulfur atoms, a soft base, within the nanopores enabled a nanoconfinement effect to selectively target Pd(II), a soft acid, to achieve the highest Pd(II) capture capacity reported to date. Moreover, chemical stability of CITCFs along with the homogeneous distribution of binding sites within the hierarchically porous polymer network enabled selective and extremely fast recovery of Pd(II) under harsh acidic and practical conditions from the mixtures of transition metals and Pd/Pt. In order to utilize the captured Pd(II) in CITCFs, a subsequent reduction was performed to form Pd nanoparticles, leading to a highly efficient heterogeneous catalyst for the Suzuki-Miyaura coupling reaction. These results clearly demonstrate the potential of POPs in the recovery of precious metals and their utilization as heterogeneous catalysts. In a broader context, this study underlines the structural tunability of POPs to achieve control over the textural properties along with the heteroatom content to target and capture different metals and to form heterogeneous catalysts for various chemical transformations, thus providing critical insights for the design of new POPs toward this end.

## EXPERIMENTAL PROCEDURES

### Resource availability

#### *Lead contact*

Further information and requests for resources should be directed to and will be fulfilled by the lead contact, Ali Coskun (ali.coskun@unifr.ch).

#### *Materials availability*

None of the unique materials generated in this study are readily available.

#### *Data and code availability*

All data needed to support the conclusions of this manuscript are included in the main text or the supplemental information. The original data of this study are openly available in Zenodo at https://doi.org/10.5281/zenodo.6589973

### Materials

All chemicals in the experimental procedures were purchased from Sigma Aldrich and used as received without further purification.

Please cite this article in press as: Song et al., Porous polyisothiocyanurates for selective palladium recovery and heterogeneous catalysis, Chem (2022), https://doi.org/10.1016/j.chempr.2022.05.009



## Characterization methods

The powder X-ray diffraction (XRD) patterns of CITCFs are collected on a Rigaku D/MAX-2500 (18 kW) micro area X-ray diffractometer using CuKα (k = 0.154 nm) radiation. The X-ray diffractograms were recorded in the 2θ range of 3°–70° with a 2θ step size of 0.15 and a step time of 1 s. The morphology of CITCFs was investigated using a field emission scanning electron microscope (FE-SEM, Tescan Mira3). Detailed analysis of various chemical bonds in each sample were probed by FTIR spectroscopy (Bruker Tensor II). XPS analysis was performed with a multi-purpose XPS (Sigma Probe, Thermo VG Scientific, X-ray source: monochromatic Al K(alpha)). Elemental analysis of CITCFs was carried out by using ThermoFischer FlashEA 2000 (Series) [C, H, N, S] Elemental Analyzer. TGA was conducted under air and $N_2$ from 25 to 1,000°C using Mettler Toledo TGA/DSC 3+ instrument. Raman analysis was conducted using WITec Raman Microscope (WITec alpha300 R, Ulm, Germany) using 532 nm laser. The textural parameters of CITCFs were evaluated by using Ar adsorption and desorption isotherms, which were measured at 77 K on a Micrometrics 3Flex Surface Characterization Analyzer. All samples were degassed at 100°C for 16 h prior to the analysis. The specific surface areas of samples were calculated using the BET and Langmuir models in the pressure range where the term $V(1 - P/P_0)$ continuously increases with $P/P_0$ in the Rouquerol plot (Figures S4and S5). The pore size distributions of samples were calculated from Ar isotherms according to NLDFT method and BJH method with Harkins and Jura thickness curve. Palladium capture study is carried out by using ICP-OES (OPTIMA7000 DV). The catalytic test for Pd@CITCF-500 is conducted using a batch reactor and analyzed with gas chromatography-mass spectrometry (GC-MS, PerkinElmer). The morphology of Pd@CITCF-500 was conducted using a FE-SEM, Tescan Mira3 and TEM, FEI Tecnai Spirit. XAS experiments were performed at the SuperXAS beamline of the Swiss Light Source at the Paul Scherrer Institute in Villigen, Switzerland.[54] The Swiss Light Source operates in top-up mode at 400 mA and 2.4 GeV. Radiation from a 2.9 T bending magnet was collimated using a Pt-coated collimating mirror at 2.84 mrad (which also served to reject higher order harmonics) subsequently monochromatized by a Si(111) channel-cut monochromator. Focusing of the beam to a spot size of 1.0 × 0.2 mm on the sample was achieved by a Pt-coated toroidal mirror. XAS spectra were collected using samples pressed to 13 mm diameter pellets formed of 40 mg of as-received sample mixed with ~20 mg cellulose. The sample measurements were performed in quick fluorescence mode using a PIPS detector.[55] Simultaneous measurement of the reference Pd foil was performed using 20 cm-long ionization chamber filled with 1 bar $N_2$ and 1 bar Ar. Spectra were collected with 1 Hz scanning speed and 300 spectra were averaged per sample. The data were processed using ProQEXAFS,[56] to calibrate, normalize and average the obtained XAS spectra with subsequent EXAFS analysis performed within the Demeter software package.[57] The amplitude reduction factor used during EXAFS refinements was obtained from fitting to the reference Pd foil and was determined to be 0.88. The liquid NMR analyses were performed on 500 MHz Bruker Avance III instrument at 298 K using deuterated solvents. The spectra were calibrated on the deuterated solvent signal. 1D $^1H$ and $^{13}C$ MAS NMR studies were conducted on Bruker 400 MHz spectrometer in 3.2 mm triple-resonance probe at the spinning rate of 16 kHz. $^1H$ NMR spectra were measured using Hahn-echo pulse sequence in 8 scans. The recycle delay was set to 1 s found as 1.3 × $T_1$, measured in saturation-recovery experiment. $^{13}C$ NMR spectra were measured using $^1H$-$^{13}C$ cross-polarization pulse sequence in 55,000–60,000 scans. The recycle delay was found and used the same way as for $^1H$ NMR spectra. 2D $^1H$ SQ-DQ correlation MAS NMR studies were conducted on Bruker 700 MHz spectrometer in 1.3 mm double-resonance probe at 50 kHz. The measurements were conducted using baba pulse sequence with the 32 transients

Please cite this article in press as: Song et al., Porous polyisothiocyanurates for selective palladium recovery and heterogeneous catalysis, Chem (2022), https://doi.org/10.1016/j.chempr.2022.05.009





in indirect and 128 scans in direct dimension with the recycle delay of 1 s. The scaling factor of 7 was used to process the indirect dimension. The $^{15}N$ dynamic nuclear polarization surface-enhanced nuclear magnetic resonance spectroscopy (DNP-SENS) experiments were performed on a Bruker 600 MHz (14.1 T) spectrometer by using a 3.2 mm HX DNP probe in $^{1}H/^{15}N$ configuration. A gyrotron generated microwaves with a power of ~6 W at 395 GHz to drive the DNP cross effect. All samples were prepared by wetness impregnation with 16 mM TEKPol solution in TCE (1,1,2,2-tetrachloroethane). Typically, for 15 mg of the sample 40 μL of radical solution was required to fully impregnate the sample; the mixture was directly packed into a 3.2 mm sapphire rotor with zirconia cap. The sapphire rotors were used for optimal microwave penetration. Rotors were inserted in the cryogenic probe within a short period of time (~5 min) and cooled to 100 K by a cryogenic heat exchanger system. In all the measurements, the MAS rate was set to 8 kHz. The spectra were recorded using $^{1}H$-$^{15}N$ CP/MAS pulse sequence with the contact time of 3 ms. The recycle delay was set to 2.5 s found as 1.3 × T1, measured in saturation-recovery experiment. The DNP enhancement of solvent (TCE) obtained was found to be 4.3, which allowed for the characterization of the samples with the natural abundance of $^{15}N$. Chemical shifts obtained in the $^{15}N$ NMR spectra were indirectly referenced by adjusting the $^{1}H$ NMR signal of TCE to 6.9 ppm. Bruker Topspin 3.2 software package was used for data acquisition and processing.

### Synthesis of covalent isothiocyanurate frameworks (CITCFs)

CITCFs were synthesized by the trimerization of 1,4-phenyl-diisothiocyanate under ionothermal conditions using $ZnCl_2$ as a reactive salt. In detail, 0.125 g of 1,4-phenyl-diisothiocyanate and 0.443 g (1:5 mole equivalent) of anhydrous $ZnCl_2$ are transferred into a Pyrex ampoule (3 × 2 cm) under an inert atmosphere. The ampoules were evacuated and sealed at room temperature. The ampoule was transferred into a box furnace and the temperature is raised to 300, 400 or 500°C (3°C $min^{-1}$ ramping) and kept under these conditions for 24 h. The ampoule was cooled to room temperature and opened carefully. Obtained dark colored CITCFs were subsequently grounded into fine powders and washed thoroughly with water to remove $ZnCl_2$. Then, the samples were stirred in a 10% HCl solution (300 mL) for 24 h and filtered. Further stirring in deionized (DI) $H_2O$ (100 mL) for 24 h and centrifugation were carried out to remove the residual salts. After the washing step, the black powder was washed successively with water, ethanol, and acetone (each 100 mL). Finally, the black powder was purified by Soxhlet washing using THF for 24 h and MeOH for 24 h. All of the samples were dried in a vacuum oven at 90°C overnight before being characterized and used further.

### Pd(II) uptake experiments

Pd mother solution (1,000 ppm) was prepared by dissolving $K_2PdCl_4$ in a deionized water. Lower concentration solutions were prepared by diluting this solution.

#### *Pd(II) adsorption isotherm*

Pd adsorption isotherm was obtained by adding 5 mg of CITCF-500 to Pd solutions (10 mL) with concentrations ranging from 3.6 to 500 ppm. The solutions were stirred overnight to reach equilibrium state and filtered using a 0.4 μm pore sized membrane filters. The filtrate phase was analyzed using ICP-OES to determine the residual metal concentration. Pd adsorption isotherm was fitted with Langmuir (Equation 1) and Freundlich (Equation 2) adsorption models:

$$q_e = \frac{Q_m k_l C_e}{1 + k_l C_e} \qquad \text{(Equation 1)}$$

Please cite this article in press as: Song et al., Porous polyisothiocyanurates for selective palladium recovery and heterogeneous catalysis, Chem (2022), https://doi.org/10.1016/j.chempr.2022.05.009



$$q_e = k_F C_e^{1/n} \quad \text{(Equation 2)}$$

where $q_e$ is the Pd uptake capacity ($mg \cdot g^{-1}$) at equilibrium, $Q_m$ is the adsorption capacity, $k_l$ is the energy of adsorption, $k_F$ and n are distribution coefficients and correction factor, respectively, and $C_e$ is the equilibrium concentration.

### *Kinetics of Pd(II) adsorption*

Pd adsorption kinetics were studied by adding 5 mg of CITCF-500 into 10 ppm Pd solution (200 mL). Several data points were obtained between 0 and 30 min by taking 3 mL aliquots from the solution (every 0.5 min). The solutions were filtered using a 0.4 μm pore sized membrane filter and the filtrate was analyzed with ICP-OES to determine the residual metal concentration. The distribution coefficient ($K_d$) is calculated by the following equation:

$$K_d = \frac{(C_o - C_e)}{C_e} \cdot \frac{V}{m} \quad \text{(Equation 3)}$$

where $C_o$ is the initial concentration, $C_e$ is the equilibrium concentration, V is volume of the solution and m is the weight of CITCF.

### *Recycling experiment of CITCF-500*

Pd recycling experiments were performed by adding 5 mg of CITCF-500 to the Pd solution (1 ppm, 100 mL) and stirring for 24 h until the equilibrium was reached. Then, the mixture was filtered to recover CITCF-500, and the filtrate was analyzed using ICP-OES. Recovered CITCF-500 is immersed into 100 mL stripping solution (2M thiourea with 2M HCl) and stirred for 24h. The CITCF-500 was filtered and washed with DI water, ethanol several times and dried in vacuum oven at 40°C for 2 h and reused in the next cycle. The CITCF-500 was fully regenerated under these conditions.

### *Pd(II) adsorption at different pH values*

The pH dependency of Pd(II) adsorption was analyzed by preparing 10 mL of 200 ppm aqueous Pd(II) solution. The pH of the solution was varied in the range of 0–12 using HCl or NaOH and monitored by a pH meter. Then, 5 mg of CITCF was added into the solution and stirred for 24 h until equilibrium was reached. The solution obtained at each pH value was filtered using a 0.4 μm pore sized membrane filter, and the filtrate was analyzed with ICP-OES to determine the residual metal concentration.

### *Selective Pd(II) adsorption from the wastewater conditioned solution*

In order to test selective Pd(II) capture from wastewater, an aqueous solution (30 mL) containing 5 ppm Pd(II), Ni(II), Zn(II), Fe(II) and Cd(II) was prepared, and then 10 mg of CITCF-500 was added to this solution and stirred overnight. The solutions were filtered using a 0.4 μm pore sized membrane filter, and the filtrate was analyzed with ICP-OES to determine the residual metal concentration.

### *Selective Pd(II) adsorption from the mixture of Pd(II) and Pt(IV)*

First, 5 ppm aqueous solution of Pd(II) and Pt(IV) (10 mL) was prepared using $K_2PdCl_4$ and $PtCl_4$ salts, respectively. pH of the solution was controlled by adding HCl. 5 mg of CITCF-500 (or CITCF-400) was added to this solution and stirred for 1 h. The solution was filtered using a 0.4 μm pore sized membrane filter, and the filtrate was analyzed with ICP-OES to determine the residual metal concentrations.

Second, 0.05 mM Pd(II) and Pt(IV) solution (10 mL) was prepared using $K_2PdCl_4$ and $PtCl_4$ salts. Then, 5 mg of CITCF-500 was added to this solution and stirred for 1h.

The solution was filtered using a 0.4 μm pore sized membrane filter, and the filtrate was analyzed with ICP-OES to determine the residual metal concentrations.

*Breakthrough experiment*

CITCF-500 sample (200 mg) was packed into a 3 cm-long HPLC column with inner diameter of 1.6 cm. Then, an aqueous solution containing 5 ppm Pd(II), Ni(II), Fe(II), Zn(II), and Cd(II) ions was prepared and passed through the column with a flow rate of 10 mL/min at room temperature. The filtrates were analyzed using ICP-OES to determine the residential metal content.

*Kinetics of Pt(IV) adsorption*

Pt(IV) adsorption kinetics were studied by adding 5 mg of CITCF-500 into 10 ppm Pt(IV) solution (200 mL). Several data points were obtained between 0 and 30 min by taking 3 mL aliquots from the solution (every 0.5 min). The solutions were filtered using a 0.4 μm pore sized membrane filter, and the filtrate was analyzed with ICP-OES to determine the residual metal concentration. The distribution coefficient ($K_d$) was calculated by using the Equation 3.

*Pt(IV) adsorption at different pH values*

pH dependency of Pt(IV) adsorption was analyzed by preparing 10 mL of 200 ppm aqueous Pt(IV) solution. The pH of the solution was adjusted in the range of 0–12 using HCl or NaOH and monitored by a pH meter. Then, 5 mg of CITCF-500 was added into the solution and stirred for 24 h until equilibrium was reached. The solution obtained at each pH value was filtered using a 0.4 μm pore sized membrane filter, and the filtrate was analyzed with ICP-OES to determine the residual metal concentration.

**General procedure for Suzuki-Miyaura coupling reaction**

Catalyst preparation: Pd(II)@CITCF-500 prepared with a Pd(II) content of 450 mg $g^{-1}$. Pd@CITCF-500 was prepared by stirring 50 mg of Pd(II)@CITCF-500 in 3 mL of 2 M aqueous $NaBH_4$ solution for 3 h at room temperature. The resulting catalysts were washed with 200 mL DI water 3 times and dried in the vacuum oven at 90°C for 3 h.

A mixture of Pd@CITCF-500 catalyst (10 mg), halobenzene (0.5 mmol), R-phenyl boronic acid (0.75 mmol) in DMF/$H_2O$ (3.5 / 3.5 mL) was stirred at 130°C for the required time to achieve highest conversion under air atmopshere. The reaction was monitored by GC-MS. After the reaction was completed, the mixture was cooled down to room temperature, diluted with ethyl acetate (15 mL), and filtered to recover the Pd@CITCF-500. The filtrate was analyzed by using GC-MS to calculate the conversion yields. For the recycling experiments, separated Pd@CITCF-500 was washed with ethyl acetate, tetrahydrofuran, and DI water several times and re-activated in the vacuum oven at 70°C for 12 h. Then, the catalyst was reused directly in the next reaction.

## SUPPLEMENTAL INFORMATION

Supplemental information can be found online at https://doi.org/10.1016/j.chempr.2022.05.009.

## ACKNOWLEDGMENTS

This publication was created as part of NCCR Catalysis (grant number 180544), a National Centre of Competence in Research funded by the Swiss National Science Foundation. A.V.Y and C.C. gratefully acknowledge ETH+ Project SynthMatLab

for the financial support. We would like to thank Mr. Patrick W. Fritz (UniFr) and Dr. Daniel Francis Abbott (ETH Zurich) for XPS measurements. We also would like to thank Mr. Indradip Mandal for the MALDI-TOF analysis.

## AUTHOR CONTRIBUTIONS

K.S.S. and S.N.T. synthesized and characterized all the polymers. K.S.S. performed Pd uptake experiments and catalytic tests. T.A. synthesized the model compounds, performed TEM and SEM analyses, and assisted with data analysis and interpretation. A.H.C. and M.N. performed EXAFs analysis and data interpretation. A.V.Y. and C.C. performed solid-state NMR analyses and data interpretation. A.C. conceived and supervised the project, procured funds, and wrote the manuscript together with all authors.

## DECLARATION OF INTERESTS

A.C. is a member of the advisory board of CHEM.

Received: September 7, 2021
Revised: October 7, 2021
Accepted: May 12, 2022
Published: June 7, 2022

## REFERENCES

1. Graedel, T.E., Harper, E.M., Nassar, N.T., Nuss, P., and Reck, B.K. (2015). Criticality of metals and metalloids. Proc. Natl. Acad. Sci. USA *112*, 4257–4262. https://doi.org/10.1073/pnas.1500415112.

2. Dumas, A., and Couvreur, P. (2015). Palladium: a future key player in the nanomedical field? Chem. Sci. *6*, 2153–2157. https://doi.org/10.1039/C5SC00070J.

3. Doronina, M.S., Karpov, Y.A., and Baranovskaya, V.B. (2017). Advanced techniques for sample processing of the reusable metal-containing raw material (Review). Inorg. Mater. *53*, 1391–1398. https://doi.org/10.1134/S0020168517140035.

4. Xolo, L., Moleko-Boyce, P., Makelane, H., Faleni, N., and Tshentu, Z.R. (2021). Status of recovery of strategic metals from spent secondary products. Minerals *11*, 673. https://doi.org/10.3390/min11070673.

5. Ruiz-Castillo, P., and Buchwald, S.L. (2016). Applications of palladium-catalyzed C–N cross-coupling reactions. Chem. Rev. *116*, 12564–12649. https://doi.org/10.1021/acs.chemrev.6b00512.

6. Johansson Seechurn, C.C.C., Kitching, M.O., Colacot, T.J., and Snieckus, V. (2012). Palladium-catalyzed cross-coupling: A historical contextual perspective to the 2010 Nobel Prize. Angew. Chem. Int. Ed. Engl. *51*, 5062–5085. https://doi.org/10.1002/anie.201107017.

7. McCarthy, S., Braddock, D.C., and Wilton-Ely, J.D.E.T. (2021). Strategies for sustainable palladium catalysis. Coord. Chem. Rev. *442*, 213925. https://doi.org/10.1016/j.ccr.2021.213925.

8. Jiang, J., Ding, W., Li, W., and Wei, Z. (2020). Freestanding single-atom-layer Pd-based catalysts: oriented splitting of energy bands for unique stability and activity. Chem *6*, 431–447. https://doi.org/10.1016/j.chempr.2019.11.003.

9. Adams, B.D., and Chen, A. (2011). The role of palladium in a hydrogen economy. Mater. Today *14*, 282–289. https://doi.org/10.1016/S1369-7021(11)70143-2.

10. Ashirov, T., and Coskun, A. (2021). Ultrahigh Permeance Metal Coated Porous Graphene Membranes with Tunable Gas Selectivities. Chem. *7*, 2385–2394. https://doi.org/10.1016/j.chempr.2021.06.005.

11. Metal cost searched result. https://www.monex.com/.

12. Glaister, B.J., and Mudd, G.M. (2010). The environmental costs of platinum–PGM mining and sustainability: is the glass half-full or half-empty? Miner. Eng. *23*, 438–450. https://doi.org/10.1016/j.mineng.2009.12.007.

13. Nuss, P., and Eckelman, M.J. (2014). Life cycle assessment of metals: a scientific synthesis. PLoS One *9*, e101298. https://doi.org/10.1371/journal.pone.0101298.

14. Ruhela, R., Singh, A.K., Tomar, B.S., and Hubli, R.C. (2014). Separation of palladium from high level liquid waste – a review. RSC Adv. *4*, 24344–24350. https://doi.org/10.1039/C4RA02024C.

15. Baba, Y., and Inoue, K. (1988). The kinetics of solvent extraction of palladium (II) from acidic chloride media with sulfur-containing extractants. Ind. Eng. Chem. Res. *27*, 1613–1620. https://doi.org/10.1021/ie00081a010.

16. Loreti, M.A.P., Reis, M.T.A., Ismael, M.R.C., Staszak, K., and Wieszczycka, K. (2021). Effective Pd (II) carriers for classical extraction and pseudo-emulsion system. Sep. Purif. Technol. *265*, 118509. https://doi.org/10.1016/j.seppur.2021.118509.

17. Wilson, A.M., Bailey, P.J., Tasker, P.A., Turkington, J.R., Grant, R.A., and Love, J.B. (2014). Solvent extraction: the coordination chemistry behind extractive metallurgy. Chem. Soc. Rev. *43*, 123–134. https://doi.org/10.1039/C3CS60275C.

18. Wang, J., Xu, W., Liu, H., Yu, F., and Wang, H. (2021). Extractant structures and their performance for palladium extraction and separation from chloride media: a review. Miner. Eng. *163*, 106798. https://doi.org/10.1016/j.mineng.2021.106798.

19. Dogan, N.A., Hong, Y., Ozdemir, E., and Yavuz, C.T. (2019). Nanoporous polymer microspheres with nitrile and amidoxime functionalities for gas capture and precious metal recovery from E-waste. ACS Sustainable Chem. Eng. *7*, 123–128. https://doi.org/10.1021/acssuschemeng.8b05490.

20. Li, X., Ma, W., Li, H., Zhang, Q., and Liu, H. (2020). Sulfur-functionalized metal-organic frameworks: synthesis and applications as advanced adsorbents. Coord. Chem. Rev. *408*, 213191. https://doi.org/10.1016/j.ccr.2020.213191.

21. Garai, M., Mahato, M., Hong, Y., Rozyyev, V., Jeong, U., Ullah, Z., and Yavuz, C.T. (2021). Asynchronous double Schiff base formation of pyrazole porous polymers for selective Pd recovery. Adv. Sci. (Weinh) *8*, 2001676. https://doi.org/10.1002/advs.202001676.

22. Hong, Y., Thirion, D., Subramanian, S., Yoo, M., Choi, H., Kim, H.Y., Stoddart, J.F., and Yavuz, C.T. (2020). Precious metal recovery from electronic waste by a porous porphyrin polymer. Proc. Natl. Acad. Sci. USA *117*, 16174–16180. https://doi.org/10.1073/pnas.2000606117.

Please cite this article in press as: Song et al., Porous polyisothiocyanurates for selective palladium recovery and heterogeneous catalysis, Chem (2022), https://doi.org/10.1016/j.chempr.2022.05.009



23. Nguyen, T.S., Hong, Y., Dogan, N.A., and Yavuz, C.T. (2020). Gold recovery from e-waste by porous porphyrin–phenazine network polymers. Chem. Mater. *32*, 5343–5349. https://doi.org/10.1021/acs.chemmater.0c01734.

24. Aguila, B., Sun, Q., Cassady, H.C., Shan, C., Liang, Z., Al-Enizic, A.M., Nafadyc, A., Wright, J.T., Meulenberg, R.W., and Ma, S. (2020). A porous organic polymer nanotrap for efficient extraction of palladium. Angew. Chem. Int. Ed. *59*, 19618–19622. https://doi.org/10.1002/anie.202006596.

25. Sharma, S., Krishna Kumar, A.S.K., and Rajesh, N. (2017). A perspective on diverse adsorbent materials to recover precious palladium and the way forward. RSC Adv. *7*, 52133–52142. https://doi.org/10.1039/C7RA10153H.

26. Slater, A.G., and Cooper, A.I. (2015). Porous materials. Function-led design of new porous materials. Science *348*, aaa8075. https://doi.org/10.1126/science.aaa8075.

27. Zou, L., Sun, Y., Che, S., Yang, X., Wang, X., Bosch, M., Wang, Q., Li, H., Smith, M., Yuan, S., et al. (2017). Porous organic polymers for post-combustion carbon capture. Adv. Mater. *29*, 1700229. https://doi.org/10.1002/adma.201700229.

28. Subramanian, S., Oppenheim, J., Kim, D., Nguyen, T.S., Silo, W.M.H., Kim, B., Goddard, W.A., III, and Yavuz, C.T. (2019). Catalytic non-redox carbon dioxide fixation in cyclic carbonates. Chem *5*, 3232–3242. https://doi.org/10.1016/j.chempr.2019.10.009.

29. Kaur, P., Hupp, J.T., and Nguyen, S.T. (2011). Porous organic polymers in catalysis: opportunities and challenges. ACS Catal. *1*, 819–835. https://doi.org/10.1021/cs200131g.

30. Zhang, Y., and Riduan, S.N. (2012). Functional porous organic polymers for heterogeneous catalysis. Chem. Soc. Rev. *41*, 2083–2094. https://doi.org/10.1039/C1CS15227K.

31. Zheng, B., Lin, X., Zhang, X., Wu, D., and Matyjaszewski, K. (2020). Emerging functional porous polymeric and carbonaceous materials for environmental treatment and energy storage. Adv. Funct. Mater. *30*, 1907006. https://doi.org/10.1002/adfm.201907006.

32. Byun, Y., Je, S.H., Talapaneni, S.N., and Coskun, A. (2019). Advances in porous organic polymers for efficient water capture. Chemistry *25*, 10262–10283. https://doi.org/10.1002/chem.201900940.

33. Je, S.H., Buyukcakir, O., Kim, D., and Coskun, A. (2016). Direct utilization of elemental sulfur in the synthesis of microporous polymers for natural gas sweetening. Chem *1*, 482–493. https://doi.org/10.1016/j.chempr.2016.08.003.

34. Chang, Z., Zeng, L., Sun, C., Zhao, P., Wang, J., Zhang, L., Zhu, Y., and Qi, X. (2021). Adsorptive recovery of precious metals from aqueous solution using nanomaterials – A critical review. Coord. Chem. Rev. *445*, 214072. https://doi.org/10.1016/j.ccr.2021.214072.

35. Zhou, L., Liu, J., and Liu, Z. (2009). Adsorption of platinum(IV) and palladium(II) from aqueous solution by thiourea-modified chitosan microspheres. J. Hazard. Mater. *172*, 439–446. https://doi.org/10.1016/j.jhazmat.2009.07.030.

36. Kuhn, P., Antonietti, M., and Thomas, A. (2008). Porous, covalent triazine-based frameworks prepared by Ionothermal synthesis. Angew. Chem. Int. Ed. Engl. *47*, 3450–3453. https://doi.org/10.1002/anie.200705710.

37. Kuhn, P., Forget, A., Su, D., Thomas, A., and Antonietti, M. (2008). From microporous regular frameworks to mesoporous materials with ultrahigh surface area: dynamic reorganization of porous polymer networks. J. Am. Chem. Soc. *130*, 13333–13337. https://doi.org/10.1021/ja803708s.

38. Rao, C.N.R., Venkataraghavan, R., and Kasturi, T.R. (1964). Contribution to the infrared spectra of organosulphur compounds. Can. J. Chem. *42*, 36–42. https://doi.org/10.1139/v64-006.

39. Rao, C.N.R., and Venkataraghavan, R. (1989). The C=S stretching frequency and the "– N–C= S bands" in the infrared. Spectrochim. Acta A Mol. Biomol. Spectrosc. *45*, 299–305. https://doi.org/10.1016/S0584-8539(89)80280-6.

40. Ferrari, A.C., Meyer, J.C., Scardaci, V., Casiraghi, C., Lazzeri, M., Mauri, F., Piscanec, S., Jiang, D., Novoselov, K.S., Roth, S., and Geim, A.K. (2006). Raman spectrum of graphene and graphene layers. Phys. Rev. Lett. *97*, 187401. https://doi.org/10.1103/PhysRevLett.97.187401.

41. Walton, R.A. (1980). The x-ray photoelectron spectra of metal complexes of sulfur-containing ligands: sulfur 2p binding energies. Coord. Chem. Rev. *31*, 183–220. https://doi.org/10.1016/S0010-8545(00)80449-X.

42. Kazansky, L.P., Pronin, Y.E., and Arkhipushkin, I.A. (2014). XPS study of adsorption of 2-mercaptobenzothiazole on a brass surface. Corros. Sci. *89*, 21–29. https://doi.org/10.1016/j.corsci.2014.07.055.

43. Rossini, A.J. (2018). Materials characterization by dynamic nuclear polarization-enhanced solid-state NMR spectroscopy. J. Phys. Chem. Lett. *9*, 5150–5159. https://doi.org/10.1021/acs.jpclett.8b01891.

44. Buyukcakir, O., Je, S.H., Talapaneni, S.N., Kim, D., and Coskun, A. (2017). Charged covalent triazine frameworks for CO2 capture and conversion. ACS Appl. Mater. Interfaces *9*, 7209–7216. https://doi.org/10.1021/acsami.6b16769.

45. Ho, Y.S. (2006). Review of second-order models for adsorption systems. J. Hazard. Mater. *136*, 681–689. https://doi.org/10.1016/j.jhazmat.2005.12.043.

46. Adams, D.M., and Cornell, J.B. (1967). Metal–sulphur vibrations. Part I. Far-infrared spectra of some complexes of thiourea and ethylenethiourea (imidazolidine-2-thione). J. Chem. Soc. A, 884–889. https://doi.org/10.1039/J19670000884.

47. Best, S.A., Brant, P., Feltham, R.D., Rauchfuss, T.B., Roundhill, D.M., and Walton, R.A. (1977). X-ray photoelectron spectra of inorganic molecules. 18. Observations on sulfur 2p binding energies in transition metal complexes of sulfur-containing ligands. Inorg. Chem. *16*, 1976–1979. https://doi.org/10.1021/ic50174a030.

48. Briggs, D., and Seah, M.P. (1993). Practical Surface Analysis, Second Edition (John Wiley & Sons).

49. Barr, T.L. (1991). Recent advances in x-ray photoelectron spectroscopy studies of oxides. J. Vac. Sci. Technol. *9*, 1793–1805. https://doi.org/10.1116/1.577464.

50. Shannon, R.D. (1976). Revised effective ionic radii and systematic studies of interatomic distances in halides and chalcogenides. Acta Cryst. A *32*, 751–767. https://doi.org/10.1107/S0567739476001551.

51. Ruiz, M., Sastre, A.M., and Guibal, E. (2000). Palladium sorption on glutaraldehyde-crosslinked chitosan. React. Funct. Polym. *45*, 155–173. https://doi.org/10.1016/S1381-5148(00)00019-5.

52. Hong, K., Sajjadi, M., Suh, J.M., Zhang, K., Nasrollahzadeh, M., Jang, H.W., Varma, R.S., and Shokouhimehr, M. (2020). Palladium nanoparticles on assorted nanostructured supports: applications for Suzuki, Heck, and Sonogashira cross-coupling reactions. ACS Appl. Nano Mater. *3*, 2070–2103. https://doi.org/10.1021/acsanm.9b02017.

53. Mitchell, S., Vorobyeva, E., and Pérez-Ramírez, J. (2018). The multifaceted reactivity of single-atom heterogeneous catalysts. Angew. Chem. Int. Ed. Engl. *57*, 15316–15329. https://doi.org/10.1002/anie.201806936.

54. Müller, O., Nachtegaal, M., Just, J., Lützenkirchen-Hecht, D., and Frahm, R. (2016). Quick-EXAFS setup at the SuperXAS beamline for in situ X-ray absorption spectroscopy with 10 ms time resolution. J. Synchrotron Radiat. *23*, 260–266. https://doi.org/10.1107/S1600577515018007.

55. Clark, A.H., Steiger, P., Bornmann, B., Hitz, S., Frahm, R., Ferri, D., and Nachtegaal, M. (2020). Fluorescence-detected quick-scanning X-ray absorption spectroscopy. J. Synchrotron Radiat. *27*, 681–688. https://doi.org/10.1107/S1600577520002350.

56. Clark, A.H., Imbao, J., Frahm, R., and Nachtegaal, M. (2020). ProQEXAFS: a highly optimized parallelized rapid processing software for QEXAFS data. J. Synchrotron Radiat. *27*, 551–557. https://doi.org/10.1107/S1600577519017053.

57. Ravel, B., and Newville, M. (2005). ATHENA, ARTEMIS, HEPHAESTUS: data analysis for X-ray absorption spectroscopy using IFEFFIT. J. Synchrotron Radiat. *12*, 537–541. HEPHAESTUS. https://doi.org/10.1107/S0909049505012719.